Nanoscale

PAPER

View Article Online
View Journal | View Issue

Cite this: *Nanoscale*, 2025, **17**, 846

A flexible and energy independent fluorescence radiation fiber film dosimeter fabricated by electrostatic spinning†

Mingshuo Tang, Zhiwei He, Zhihao Wang and Yunlong Wang *

Received 18th August 2024,
Accepted 13th November 2024

DOI: 10.1039/d4nr03392b

rsc.li/nanoscale

Doping fluorescent substances in polymer matrices has shown promising applications in radiation dose sensing. In this work, quinoline dye based polyvinyl chloride fibrous films with fiber diameters of 123 nm, 540 nm and 864 nm were obtained by electrostatic spinning. The introduction of the fiber film structure makes the fluorescent film dosimeter flexible and lightweight compared to normal solid fluorescent films and further extends the linear range of X-ray detection to 0–350 Gy. Furthermore, the dosimeter shows energy and dose rate independence, and the sensitivity of the dosimeter can be improved by the application of fiber films with thinner diameters. This flexible fiber membrane provides a candidate material for wearable visual dosimeters.

Introduction

X-rays have been widely used in medical treatment, industrial testing, sterilization, security screening and scientific research since being discovered by Roentgen in 1895, and radiation protection against the concomitant harm from X-rays has always been a critical issue.[1,2] Thus, quantifying the dose of X-rays is necessary, especially when they are applied for tumor radiotherapy, where the cumulative irradiation dose delivered to the target tissue can reach 50 Gy.[3,4] Furthermore, many other activities of human beings, such as space exploration,[5,6] industrial CT[7,8] and flaw detection,[9] also face the threat of X-rays; thus, dosimeters have been critical tools for practitioners in related industries.

Numerous dosimeters have also been invented to accurately calibrate the dose, for instance, ionization chambers,[10] semiconductor dosimeters,[11] and chemical film dosimeters,[12] but significant efforts are still needed to achieve an ideal dosimetry system. Ionization chambers or semiconductor dosimeters provide fine accuracy and direct read-out of the dose; however, the complex power supply and electronic readout systems make their cost relatively high, and the dead time greatly impacts their accuracy and reliability when the dose rate increases.[13–15] The response of some film dosimetry systems greatly depends on the energy of X-rays, and the existing film dosimeters are solid sheets and not flexible to adapt to the surface of target surfaces.[16,17] Besides, many dosimeters such as thermoluminescent dosimeters cannot detect spatial dose distribution or require complex pretreatment, readout and calibration procedures.[18,19] Finally, commercially available personal dosimeters are not only inconvenient to observe or uncomfortable to wear, but they also struggle to adapt to the shape of the human body, hindering accurate measurement of the important areas of the body. Therefore, a flexible and wearable fluorescent X-ray dosimeter is urgently needed.[20–23] Compared to numerous other dose detection methods, fluorescence sensing has proven to be a powerful tool for detecting X-ray doses due to its high sensitivity, real-time performance,

College of Materials Science and Technology, Nanjing University of Aeronautics and Astronautics, Nanjing 211106, P. R. China. E-mail: wylong@nuaa.edu.cn

†Electronic supplementary information (ESI) available. See DOI: https://doi.org/10.1039/d4nr03392b

Yunlong Wang

Dr Yunlong Wang obtained his B.S. degree in 2009 and Ph. D. in 2015, both from the University of Science and Technology of China. He has previously worked at the Institute of Nuclear Physics and Chemistry, China Academy of Engineering Physics, and the Shenzhen Institute of Advanced Technology, Chinese Academy of Sciences and is currently employed at the Nanjing University of Aeronautics and Astronautics as an Associate Professor (Principal Investigator). His research focused on radiation dosimeters based on soft smart materials, radiation synthesis of soft smart materials, and the characterization of smart materials using nuclear techniques such as neutron scattering.

low cost and convenient visualization.[24,25] In addition, proportional fluorescence sensing measures the change in fluorescence intensity and the ratio of two different wavelengths, which is dependent on processes such as intramolecular charge transfer (ICT),[26] excited state intramolecular proton transfer (ESIPT), *etc*., and has the advantage of self-intensity calibration.

In recent years, polymer fluorescent films have emerged as promising dosimeters because of the advantages of high sensitivity, ease of fabrication, and good flexibility.[27–29] After X-ray irradiation, the color of these films' fluorescence was found to change in the visible region, which can be easily differentiated by the naked eye with the help of a black light UV lamp, providing an ideal candidate for wearable dosimeters. For instance, Zhang *et al.*[30] recently designed a pH-sensitive fluorescent quinoline derivative with a significant shift from blue to red spectra after acidification. They found that the H^+ ions generated by poly(methyl methacrylate) (PMMA) and poly(vinyl chloride) (PVC) under γ-ray irradiation can trigger this shift, and the fluorescence intensity ratio of two fixed wavelengths ($I_{585\ nm}/I_{468\ nm}$) has a linear response to the absorbed dose over a wide dose range (80–4060 Gy). However, the stiff and solid films are not suitable for wearable dosimeters, and the dependence on proton energy remains unclear.

In recent years, as the demand for flexible dosimeters has increased polymer fiber films have been gradually proposed to serve as the carrier of radiation dosimeters to improve their shape adaptability.[31–34] The first type of fiber film dosimeter is based on PCDA, a radiochromic reagent that darkens its color through radiation-induced polymerization. For instance, Qi *et al.*[31] prepared a PEO/PCDA nanofiber fiber film using an electrostatic spinning technique and proved that the absorbance remains linear with the variation in absorbed doses, and the sensitivity of the dosimeter also showed a linear increasing trend with the increase in the PCDA content. Vo *et al.*[35] successfully prepared a PCDA-based PLA composite fiber dosimeter using centrifugal spinning and achieved an X-ray absorbed dose detection range of 2.2–40 Gy. The composite fiber film changed from white to dark blue after X-ray irradiation in the range of 2.2–15.0 Gy and the increase of ΔE showed pseudo-linear behavior. In the dose range of 15.0–40.0 Gy, the chromaticity difference variation is almost saturated and the detection range is relatively narrow. Fiber films were also applied in fluorescent radiation dosimeters; for instance, Al-Hazmy *et al.*[36] found that the irradiation of γ-rays (dose = 420 mR) caused the disappearance of a resolved Franck–Condon fluorescence peak at 561 nm and a blue shift of 4 nm on the DBDMA-doped fiber film, while only increasing the emission intensity with an ordinary thin layer film, thus providing a potent candidate as an efficient sensor for dosimetric devices. These findings confirmed fiber films can serve as carriers of radiation-sensitive materials and provide additional benefits.[37] As reported in many literature studies, electrostatic spinning is a technique capable of producing uniform nanofibers, and the properties of fibers can be easily tuned through parameters that are applied in the spinning process, for instance, the voltage, concentration of the polymer solution, and the feeding rate.[38–41] In the electrostatic spinning process, the polymer in the spinning solution is driven by an electric field force. When the voltage reaches a critical value, the charged part of the solution forms a jet stream and splits.[42–44] After evaporation of the solvent and curing of the fibers, the film of nanofibers with a uniform diameter is finally obtained at the winding device. Compared to ordinary spinning techniques such as dry spinning and wet spinning, electrostatic spinning avoids the poor dispersity of produced fibers.[45,46]

In order to prepare a flexible fluorescence film radiation dosimeter, highly sensitive fluorescence that responds to radiation is needed, and a pH-responsive organic quinoline fluorophore dye (QFD) which was reported by Pei and coworkers was selected in the current work.[30] The QFD was synthesized following their previous report. The QFD can work as a ratiometric probe, providing a quantitative response to the concentration of H^+ ions produced by PVC after high energy irradiation. The single-component fluorescent quinolinophore provides a convenient detection method for high-energy radiation with better reproducibility than traditional ratiometric sensing composed of two or more dyes. However, a deviation from linear relationship and inhomogeneity were obviously observed from the reported results.

In this paper, homogeneous PVC fiber films based on fluorescent quinolinophores are prepared *via* electrostatic spinning methods proposed for the detection of X-ray doses. The changes in fluorescence spectra were investigated when the film was irradiated by X-ray doses, as well as the visible color shift of the fluorescence from blue to red. The fluorescence intensities of the emission peaks in the blue region and the emission peaks in the red region were measured, and then a linear relationship was established between the X-ray dose and the intensity ratio (I_{red}/I_{blue}). The energy and dose rate dependence of the dosimetric film was also investigated, to verify its versatility as an X-ray radiation dosimeter. Using the nanofiber film dosimeter prepared by electrostatic spinning, the flexibility was significantly increased. Furthermore, we found that not only the sensitivity but also the dose detection range of the dosimeter was improved since the formation of a fiber film greatly decreased the self-absorption effect. The effect of the diameter of the fibers generated by electrostatic spinning on the sensitivity was also investigated by increasing the fiber diameter in the nanometer range. Besides, the preparation of the fiber film greatly enhanced the flexibility and shape adaptability of the fluorescent radiation dosimetric film, providing a candidate for wearable visual dosimeters.

Results and discussion

As shown in Fig. S1,† the QFD was successfully synthesized following the previous literature[30] and was verified using ^{1}H-NMR characterization. The QFD was co-dissolved with PVC in tetrahydrofuran and then injected into the template to evaporate the solvent at room temperature to form a homogeneous

solid fluorescent film. The obtained film is placed in a vacuum oven to further remove the residual solvent. The PVC films exhibit blue fluorescence under 365 nm UV excitation, and the photoluminescence color changes from blue to red when the films are irradiated with X-rays at a dose rate of 4.98 Gy min^{-1} for 13 different doses (14.94–373.5 Gy). Fig. 1a illustrates the mechanism by which QFD responds to X-ray irradiation. The fluorescent dye-doped PVC film shows a fluorescence emission with the intensity peaking at ~484 nm (λ_{em}) under 420 nm light excitation, while the emission in the red region can be neglected. When the X-ray dose increases, a distinct peak appears at ~570 nm, while the fluorescence intensity in the blue region decreases and the wavelength of its emission peak exhibits a blue shift (λ_{em} = 478 nm). As shown in Fig. 1b, the visible fluorescence color of the composite film shifted from blue to red gradually. As shown in Fig. 1c and d, when the X-ray dose increased gradually from 0 to 124.5 Gy, the ratio of the emission peak in the red region to that in the blue region shows a linear increase trend with a coefficient of determination of linear fitting (R^2) of 0.98, but deviates from the linear relationship obviously after the dose continues to increase. Except for the improved homogeneity of the film dosimeter induced by the electrospinning technique, the decrease of the self-absorption also expands the linear response region of the dosimeter. As shown in Fig. S2,† the UV-vis absorbance of the solid fluorescent films before and after irradiation was recorded. When irradiated with X-rays, the fluorescence dye dissolved in the solid film shows an increase in absorbance in the visible light band region except for the red-light region. Therefore, I_{blue} was reduced by the self-absorption in the solid film, while I_{red} was not weakened. The ratio of I_{red}/I_{blue} increases accordingly and deviates from the linear law. When the dosimeter is fabricated into fiber films with electrostatic spinning, the thickness of the matrix reaches sub-micrometers and greatly decreases the self-absorption effect, therefore expanding the linear region when the absorbed dose exceeds 124.5 Gy. At a dose of 373.5 Gy, the red fluorescence spectrum (λ_{em} = 604 nm) occupies almost the entire fluorescence spectrum, and the emission peaks in the blue region are almost invisible. The shift of the fluorescence emission peak is attributed to the production of protons from X-ray irradiation of the PVC substrate (Fig. 1a), and the induced $H^{\bullet}$ binding to $Cl^{\bullet}$ can produce HCl, as reported in previous literature.[30] Due to the combination of H^+ with the electron pair on the N atom of the quinoline group, the binding at this site enhances the charge transfer in the quinoline ring; therefore, the emission in the red region increases gradually, while the emission in the blue region decreases respectively.

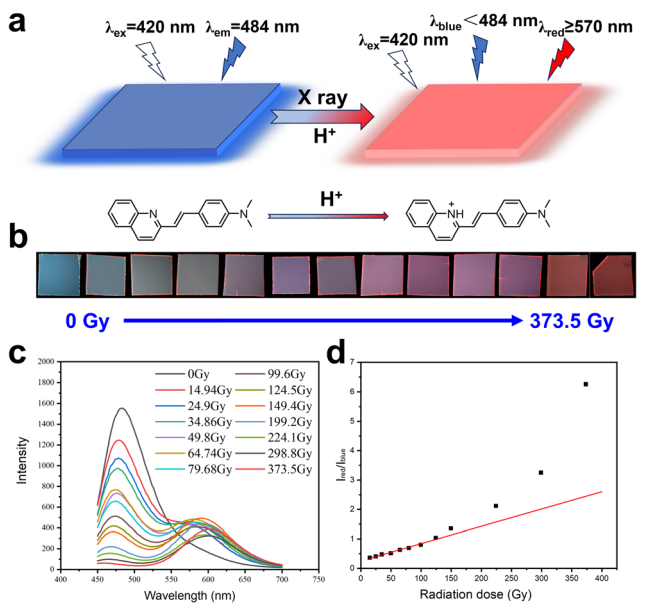

Fig. 1 Fabrication and radiation response of solid QFD films without the fiber structure. (a) Schematic illustration of QFD's visual sensing of X-ray irradiation by QFD/PVC composite films. (b) Photographs of QFD (0.1 wt%) in PVC after exposure to different X-ray doses under 365 nm UV excitation. (c) Steady-state emission spectra of QFD (0.1 wt%) in PVC under 420 nm light excitation after exposure to different doses of X-rays. (d) Linear fitting relationship between the fluorescence intensity ratio (I_{red}/I_{blue}) and absorbed X-ray doses.

An ideal dosimeter should be energy or dose-rate independent. To probe the energy dependence of the film, the composite film was irradiated at different high voltages of 20 kV, 60 kV and 140 kV with an X-ray tube while maintaining a tube current of 2 mA. The photoluminescence spectra after X-ray irradiation are shown in Fig. 2a–c. To probe the dose rate dependence of the films, the irradiation was performed at dose rates of 4.98 Gy min^{-1} and 19.3 Gy min^{-1} at a high voltage of 140 kV, respectively. The photoluminescence spectra after X-ray irradiation are shown in Fig. 2c and d. The ratio of fluorescence intensity between the red region emission peaks and the blue region emission peaks (I_{red}/I_{blue}) was linearly correlated with the received X-ray dose as shown in Fig. 2e and f respectively, indicating that energy and the dose rate had no significant effect on the fluorescence film dosimetric system. Therefore, the QFD/PVC composite film can behave as an energy and dose rate independent radiation system below 125 Gy, but deviates from the linear relationship obviously after the dose continues to increase. Besides, the lack of flexibility is also a factor that limits its widespread application. Thus, electron spinning was applied with the QFD/PVC composite radiation system to address these issues.

In the process of electrostatic spinning, the diameter of PVC nanofibers depends on the concentration of the spinning solution and various parameters of electrostatic spinning (voltage, distance, temperature, humidity, rotational speed, *etc.*). Therefore, the effect of spinning liquid concentration and the voltage level on the fiber diameter is investigated. Fig. 3 shows the SEM images of PVC fibers with two concentrations of 10% and 15% at a spinning voltage of 15 kV, a spinning distance of 14 cm and a fluorescent dye concentration of 1‰. As shown in Fig. 3a and b, uniform fibers were successfully prepared under the above conditions. When the concentration of the spinning solution was increased from 10% to 15%, the fiber diameter increased significantly and the

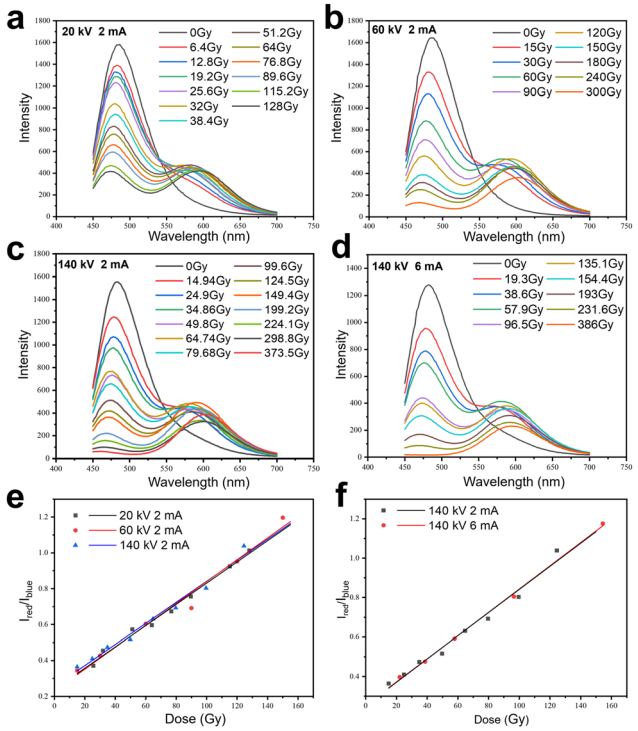

Fig. 2 Energy dependence of QFD films as an X-ray radiation detection material. (a–c) Steady-state emission spectra of QFD (0.1 wt%) in PVC under 420 nm light excitation after irradiation with different doses of X-rays at tube voltages of 20 kV, 60 kV, and 140 kV and a tube current of 2 mA. (d) Steady-state emission spectra of QFD (0.1 wt%) in PVC under 420 nm light excitation after irradiation with different doses of X-rays at a tube voltage of 140 kV and a tube current of 6 mA. (e) The linear fitting relationship between the fluorescence intensity ratio (I_{red}/I_{blue}) and the irradiated X-ray dose at different energies. (f) The linear fitting relationship between the fluorescence intensity ratio (I_{red}/I_{blue}) and the absorbed X-ray dose at different dose rates.

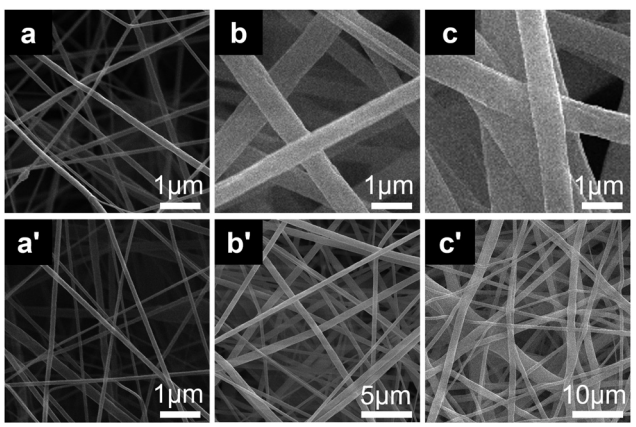

Fig. 3 SEM photographs of QFD-doped PVC fiber films at different precursor concentrations and voltages in electrostatic spinning. (a, a') 10 wt%, 15 kV; (b, b') 15 wt%, 15 kV; and (c, c') 15 wt%, 10 kV.

average diameter increased from 123 nm to 540 nm, and the fibers obtained were smoother. As the concentration increases, the viscosity of the polymer jet increases, which improves the resistance to stretching by electric field forces, and thus the fiber diameter becomes coarser. In addition, the viscosity of the spinning solution is low at low concentrations. A lower concentration will induce lower polymer chain entanglement; if the entanglement continues to decrease, it will result in frequent interruptions of the polymer jet and splitting of the jet into a large number of small point-bearing droplets by electric field forces. In contrast, if the concentration exceeds the critical concentration, the pressure in the syringe will be too high to finish the spinning procedure. Therefore, the voltage is decreased to 10 kV to obtain a smooth and uniform fiber film. The SEM in Fig. 3c shows that by decreasing the voltage to 10 kV, smooth fibers with an average diameter of 864 nm were successfully prepared. The increment of the diameter of the fibers is because the charges on the polymer jet and the repulsive forces between the polymer and jet accordingly decrease as the applied voltage decreases. By tuning the above conditions, fluorescent fiber films with three different diameters, which are 123 nm, 540 nm and 864 nm, are successfully obtained.

Three fluorescent nanofiber films with different diameters (123 nm, 540 nm, and 864 nm) were prepared using electrostatic spinning and irradiated with X-rays also at a dose rate of 4.98 Gy min^{-1}. The photoluminescence spectra of these fibrous membranes irradiated with different doses of X-rays at the 420 nm excitation wavelength are shown in Fig. 4a–c. Meanwhile, in order to maintain the same conditions as the nanofiber films, we mixed quinoline dye and PVC into a solvent of THF : DMF (1 : 1), which was evaporated at room temperature and vacuum degassed to obtain a polyvinyl chloride precursor film dosimeter for comparison. The fluorescence

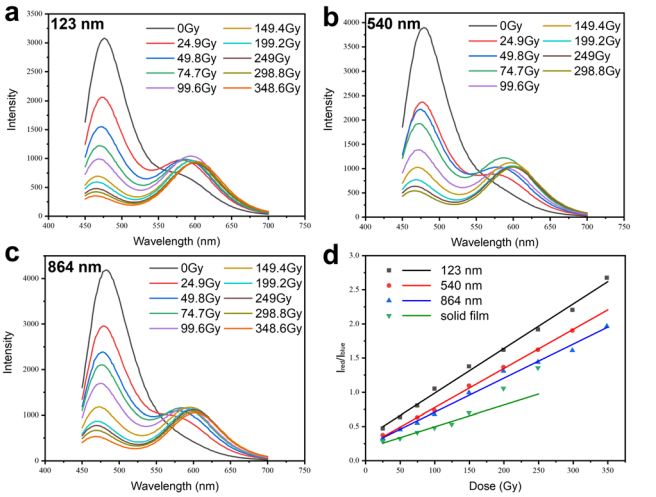

Fig. 4 Effect of fiber thickness on the radiation response of QFD fiber films. (a–c) Steady-state emission spectra of QFD (0.1 wt%) in PVC fiber films with diameters of 123 nm, 540 nm, and 864 nm under 420 nm light excitation after exposure to different doses of X-rays. (d) The linear fitting relationship between the fluorescence intensity ratio (I_{red}/I_{blue}) of the three different diameters of nanofiber films and the precursor film and the irradiation X-ray dose.

Table 1 Slope and R^2 obtained by linear fitting in Fig. 4d

	123 nm	540 nm	864 nm	Solid film
Slope	0.00653	0.00572	0.00498	0.00318
R^2	0.99488	0.99779	0.99129	0.955

intensity ratio (I_{red}/I_{blue}) of the emission peaks in the red region and the emission peaks in the blue region was linearly correlated with the absorbed X-ray dose (the fitted data are shown in Table 1). Linear response relationships were obtained for precursor film dosimeters and fiber film dosimeters of different diameters, respectively (Fig. 4d), where the X-ray dose was determined using a Fricke dosimeter. Consistent with the findings above, as shown by the green fitted straight line in Fig. 4d, we found that the polyvinyl chloride precursor fluorescent film dosimeters responded linearly only in the range of 15–150 Gy, and the fluorescence intensity ratios showed a nonlinear trend beyond 150 Gy. However, the fluorescent nanofiber film successfully maintains the linear response beyond 150 Gy and finally reaches approximately 350 Gy, far exceeding the range of the solid film dosimeter. On the other hand, as shown in Fig. 4d and Table 1, the slopes of the fitted straight lines of the three nanofiber films are larger than that of the solid film and their R^2 values are higher than that of the solid film dosimeters, which implies an increase in the sensitivity and detection range. When PVC fiber films are irradiated with X-rays, HCl is produced in the matrix. The production of this acid is related to the radiation dose. Due to the larger surface area of fibrous films, their contact area with air is increased, allowing better oxygen penetration into the material than non-fibrous membranes. Since oxygen under radiation can participate in and accelerate the radiation splitting of polymers,[47] fibrous films (with smaller diameters) can produce more acid at the same radiation dose, resulting in a stronger acid-responsive fluorescent molecule response. Accordingly, the finer the fiber, the more acid is produced. Therefore, as the diameter of the nanofibers becomes thinner, the sensitivity of the corresponding dosimeter increases. Taking I_{red}/I_{blue} = 1.6 as an example, the absorbed doses needed to reach this ratio by the fiber membranes with diameters of 123 nm, 540 nm, and 864 nm are 193 Gy, 244 Gy, and 279 Gy, respectively, and this increase in sensitivity may be attributed to the fact that the specific surface area of the fibers is inversely proportional to their diameters. The diameter of the fibers in the films may be a decisive factor in increasing the sensitivity, and the 150 nm diameter fiber film, which is the finest fiber produced in this work, causes a faster red shift of the emission peaks in the red region at the same dose of irradiation, thus obtaining the highest sensitivity in the X-ray dose detection.

We used dosimeters based on fluorescent dye nanofibers (average diameters: 123 nm and 864 nm) for fluorescence visualization experiments after X-ray exposure. The fibrous films were irradiated with different doses of X-rays and showed color changes under 365 nm UV excitation, as shown in Fig. 5a and b.

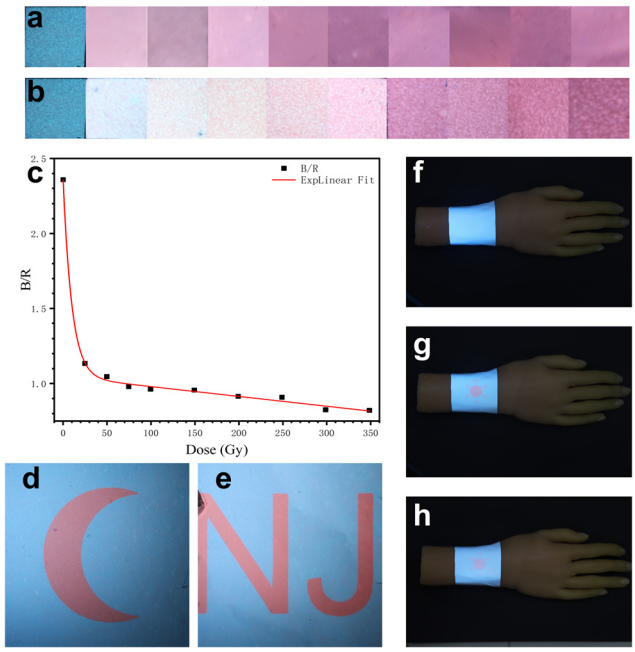

Fig. 5 Visual readout and patterning of QFD fiber dosimeters. (a) Photographs of QFDs (0.1 wt%) in 123 nm PVC fiber films after exposure to different X-ray doses under 365 nm UV excitation. (b) Photographs of QFDs (0.1 wt%) in 864 nm PVC fiber films after exposure to different X-ray doses under 365 nm UV excitation. (c) The linear fitting relationship between the B/R ratio and irradiated X-ray dose (QFD-doped 864 nm PVC fiber film). (d and e) Photograph of the QFD-doped 123 nm PVC fiber film after X-ray irradiation using a lead pattern to form "🌙" and "NJ" patterned radiation fields. (f) Photograph of the QFD-doped 123 nm PVC fiber film without X-ray irradiation. (g) Photograph of a fibre film dosimeter with a diameter of 123 nm after radiation patterning. (h) Photograph of a fiber film dosimeter with a diameter of 123 nm after irradiation patterning and storage for 7 days.

The leftmost part of Fig. 5b shows the film without X-ray irradiation with strong blue fluorescence. As the dose accumulates, the acid produced by X-ray irradiation of the PVC substrate increases, and the pH-sensitive fluorescent dyes cause a visual color change, and the photoluminescent color of the film gradually changes from blue to red and further deepens. The digital images were then processed with photo processing software to obtain RGB values, and the B/R ratio was obtained as shown in Fig. 5c. The B/R ratio showed a decrease with the absorbed doses and could be fitted as a sum of exponential decay and linear descent. Thus, the dosimetric properties of the film provide potential for dose measurement using digital photos. We placed lead plates with different patterns on top of a fluorescent nanofiber dosimeter to distinguish between X-ray exposed and unexposed areas. Then, it was placed under X-ray irradiation and the film was removed after the radiation dose reached 199.2 Gy. As shown in Fig. 5d and e, under 365 nm UV excitation, the red region indicates the X-ray exposed region of 199.2 Gy, while the blue region is the non-irradiated region, showing the spatial resolution of the dosimeter. Besides, as shown in Fig. S3a and b,† the fluorescence fiber film dosimeter shows perfect flexibility

Table 2 Comparison table between existing work and this work

	Shape	Linearity	Response region	Response method
Choudhary *et al.*[25]	Solution	Good	0–200 Gy	Ratiometric fluorescence
Pei *et al.*[30]	Solid film	Fair	0–4 kGy	Ratiometric fluorescence
Kinashi *et al.*[23]	Fiber film	Nonlinear	0–20 Gy	Color density
Vo *et al.*[35]	Fiber film	Nonlinear	0–40 Gy	Color density
Vo *et al.*[32]	Fiber film	Nonlinear	0–80 Gy	Color density
Al-Hazmy *et al.*[27]	Fiber film	N/A (single dose point)		Fluorescence shift
Wang *et al.*[24]	Solid film	Not reported	0–10 kGy	Color density
Qin *et al.*[48]	Gel	Good	0–15 Gy	Fluorescence intensity
This work	Fiber film	Good	0–350 Gy	Ratiometric fluorescence

and shape adaptability and can conveniently fit the arm model, providing spatially resolved dosimeter measurement.

The film dosimeter also shows good durability after irradiation. As shown in Fig. 5, a film dosimeter was irradiated to form a fluorescent pattern and then stored under normal conditions for 7 days after irradiation. As shown in Fig. 5f–h, the patterns on the fiber dosimeters were unchanged after 7 days after irradiation. The film dosimeter also provides mechanical properties suitable for wearable dosimeter applications. Fig. S3c and d† show the stress–strain curves of fiber film dosimeters. The maximum tensile stress and the elongation at maximum tensile stress of the fiber membrane dosimeter with a diameter of 864 nm were 5.137 MPa and 23.1%, while those of 123 nm were 1.477 MPa and 23.8%, respectively. Besides, the film has a fabric weight as light as 25 g m^{-2}, and thus has the potential to be a wearable detection device for radiation monitoring, such as dosimeters sewn onto surgical gowns or gloves for operators in interventional radiotherapy.

In order to demonstrate the advantages of fiber membrane dosimetry and the novelty of our work, a comparison table between reported work and this work is shown in Table 2. While the fiber film dosimeter inherits and increases the high sensitivity of the fluorescence dosimeter, there was also an extension of its linear response range to 0–350 Gy with improved linearity. At the same time, the color phase change provides a more intuitive display of the absorbed dose compared to these based on the fluorescence intensity or color density.

Conclusions

In summary, by introducing an electrostatic spinning generated fiber film, a flexible and energy-independent PVC fluorescence radiation fiber film dosimeter containing fluorescent quinolinophores was prepared. A linear relationship was established between the X-ray dose and the intensity ratio (I_{red}/I_{blue}), and the energy and dose rate dependence of the dosimetric film was also investigated, to verify its versatility as an X-ray radiation dosimeter. The dosimeter in the form of fiber films produced by electrostatic spinning decreases the thickness of the matrix and greatly decreases the self-absorption effect, thereby expanding the linear region. Besides, the decrease in the thickness also increases the penetration of oxygen into PVC and can increase the production of H^+ ions, making the dosimeter more sensitive. The visible color shift of the fluorescence from blue to red also provides a readout technique through the B/R ratio obtained in the digital camera. The flexibility of the fiber film makes it capable of adapting to the anatomy of the human body, and the low fabric weight makes it a candidate for wearable visual dosimeters.

Experimental section

Materials

2-Methylquinoline (purity, 98%), *p*-toluenesulfonamide (purity, 99%), *p*-dimethylaminobenzaldehyde and polyvinyl chloride were purchased from Aladdin Biochemical Technology Co. Petroleum ether and *N*,*N*-dimethylformamide (DMF) were purchased from Shanghai McLean Biochemical Technology Co. Ethanol was purchased from Sinopharm Chemical Reagent Co. Tetrahydrofuran (THF) was purchased from Nanjing Chemical Reagent Co. Ultrapure water was used in all experiments, and all chemicals were used directly without further purification.

Synthesis of fluorescent dye

2-Methylquinoline (1.43 g) and *p*-toluenesulfonamide (1.79 g) were mixed in 10 ml of toluene, heated to 120 °C and stirred for 30 min. Then *p*-dimethylaminobenzaldehyde (2.09 g) was added and the reaction was continued for 120 h at 120 °C. After the reaction, the sample was cooled to room temperature filtered and recrystallised in ethanol. The resulting sample was then further purified in a liquid chromatography column to finally obtain yellow crystals.

Preparation of polymer solutions and fiber film dosimeters

PVC powder and quinoline dye (1/1000, wt/wt) were co-dissolved in a solvent mixture of tetrahydrofuran and *N*,*N*-dimethylformamide (1/1, wt/wt), and then stirred at 50 °C for 2 hours using a magnetic stirrer. After complete dissolution, it was left at room temperature to remove air bubbles to finally obtain a homogeneous spinning solution.

Fluorescent nanofiber films were prepared using the electrostatic spinning technique and the spinning solution was formulated with a concentration of 10% and 15%, respectively. The spinning solution was injected into a 20 ml syringe

and the syringe pump was advanced at a flow rate of 5.5 ml h^{-1}. The applied voltage was 10–15 kV and the high-voltage power supply was connected to the tip of the needle using a high-voltage clamp. Aluminium foil was placed over the cylindrical collector and the distance from the tip of the needle to the collector was fixed at 10 cm. The needle was made to reciprocate at a uniform speed using a reciprocating pump to obtain a nanofiber dosimeter of uniform thickness. At the end of the winding, the fiber film was evaporated overnight at room temperature, which ensured complete evaporation of the solvent.

Characterization

Images of the morphology of electrostatically spun PVC nanofibers were obtained using a scanning electron microscope (Hitachi SU8220, Japan). The average diameter of the fibers was obtained from the SEM images using image processing software (ImageJ). Steady-state emission spectra were acquired on a microplate reader (InfiniteM200PRO) with an excitation light wavelength of 420 nm. Photographs were taken using a digital camera (Nikon D3100). Continuous X-ray radiation was generated using an X-ray tube with a Mo target and the dose rate of X-rays was measured with a Fricke dosimeter. The sample was irradiated for a certain time at room temperature and the dose rate and the time of irradiation were multiplied to obtain the absorbed dose.

Author contributions

T. M.: methodology, investigation, formal analysis, and writing – original draft; H. Z.: investigation; W. Z.: validation; W. Y.: conceptualization, funding acquisition, supervision, and writing – review & editing.

Data availability

The data supporting this article have been included in the main text and the ESI,† and any additional data related to this article are available upon request from the authors.

Conflicts of interest

There are no conflicts to declare.

Acknowledgements

This work was supported by the National Key R&D Program of China (2022YFB1902900), Natural Science Foundation of Jiangsu Province (BK20242043), National Natural Science Foundation of China (22006067), National Defense Technology Industry Nuclear Power Technology Innovation Center (HDLCXZX-2022-HD-033), Fundamental Research Funds for the Central Universities at NUAA (NZ2024038), and Postgraduate Research & Practice Innovation Program of NUAA (xcxjh20230618).

References

1 Z. Yang, J. Hu, D. Van der Heggen, M. Jiao, A. Feng, H. Vrielinck, P. F. Smet and D. Poelman, A Versatile Photochromic Dosimeter Enabling Detection of X-Ray, Ultraviolet, and Visible Photons, *Laser Photonics Rev.*, 2023, **17**(5), 2200809.
2 X. He, M. Xia, H. Wu, X. Du, Z. Song, S. Zhao, X. Chen, G. Niu and J. Tang, Quasi-2D Perovskite Thick Film for X-Ray Detection with Low Detection Limit, *Adv. Funct. Mater.*, 2022, **32**(7), 2109458.
3 Y. Xu, B. Dong, W. Zhu, J. Li, R. Huang, Z. Sun, X. Yang, L. Liu, H. He, Z. Liao, N. Guan, Y. Kong, W. Wang, J. Chen, H. He, G. Qiu, M. Zeng, J. Pu, W. Hu, Y. Bao, Z. Liu, J. Ma, H. Jiang, X. Du, J. Hu, T. Zhuang, J. Cai, J. Huang, H. Tao, Y. Liu, X. Liang, J. Zhou, G. Tao, X. Zheng and M. Chen, A Phase III Multicenter Randomized Clinical Trial of 60 Gy versus 50 Gy Radiation Dose in Concurrent Chemoradiotherapy for Inoperable Esophageal Squamous Cell Carcinoma, *Clin. Cancer Res.*, 2022, **28**(9), 1792–1799.
4 H. Hirai, T. Ohsako, T. Kugimoto, H. Tomioka, Y. Michi, K. Kayamori, T. Yoda, M. Miura, R. Yoshimura and H. Harada, Comparison of 50- and 66-Gy Total Irradiation Doses for Postoperative Cervical Treatment of Patients With Oral Squamous Cell Carcinoma, *Oral Oncol.*, 2020, **107**, 104708.
5 L. Vico and A. Hargens, Skeletal Changes During and after Spaceflight, *Nat. Rev. Rheumatol.*, 2018, **14**(4), 229–245.
6 H. Tsuchida, R. Nakamura, K. Kinashi, W. Sakai, N. Tsutsumi, M. Ozaki and T. Okabe, Radiation-induced Colour Changes in a Spiropyran/BaFCl:Eu^{2+}/Polystyrene Composite Film and Nonwoven Fabric, *New J. Chem.*, 2016, **40**(10), 8658–8663.
7 B. Nugraha, P. Verboven, S. Janssen, Z. Wang and B. M. Nicolaï, Non-Destructive Porosity Mapping of Fruit and Vegetables Using X-Ray CT, *Postharvest Biol. Technol.*, 2019, **150**, 80–88.
8 H. M. Shi, Z. C. Sun and F. H. Ju, Understanding the Harm of Low-Dose Computed Tomography Radiation to the Body (Review), *Exp. Ther. Med.*, 2022, **24**(2), 534.
9 F. Zuo, J. Liu, X. Zhao, L. Chen and L. Wang, An X-Ray-Based Automatic Welding Defect Detection Method for Special Equipment System, *IEEE/ASME Trans. Mechatron.*, 2024, **29**(3), 2241–2252.
10 H. I. Shirvanedeh, H. S. Douk and B. Farhood, Improving and Optimizing the Structure of a Cylindrical Ionization Chamber for Radiation Protection Dosimetry: Guard Electrode and Chamber Wall, *Radiat. Phys. Chem.*, 2019, **163**, 45–51.
11 J. J. Kim, J. M. Ha, H. M. Lee, H. S. Raza, J. W. Park and S. O. Cho, Effect of Electron-Beam Irradiation on Organic Semiconductor and Its Application for Transistor-Based

Dosimeters, *ACS Appl. Mater. Interfaces*, 2016, **8**(30), 19192–19196.

12 Y. S. Soliman, S. M. Tadros, W. B. Beshir, M. M. Naoum, G. R. Saad and L. I. Ali, A Radichromic Dye of Tris-(4-Aminophenyl)Methane Incorporated into Polymeric Films for Radiation Dose Monitoring, *Dyes Pigm.*, 2023, **217**, 111387.

13 Z. Yang, H. Vrielinck, L. G. Jacobsohn, P. F. Smet and D. Poelman, Passive Dosimeters for Radiation Dosimetry: Materials, Mechanisms, and Applications, *Adv. Funct. Mater.*, 2024, **34**, 2406186.

14 Y. Yan, C. Zhang, L. Zheng, T. Wang, M. Li, F. Xie, Q. Guo and G. Peng, Dosimeter Based on YAG: Ce Phosphor via Sol-Gel Method for Online X-ray Radiation Monitoring, *Crystals*, 2021, **11**(12), 1567.

15 A. Mittal, G. Natanasabapathi, A. Verma and P. Kumar, Development and Dosimetric Characterization of Novel Amide Substituted Diacetylene Based Radiochromic Films for Medical Radiation Dosimetry, *Radiat. Phys. Chem.*, 2021, **182**, 109391.

16 P. L. Roberson, J. M. Moran and R. Kulasekere, Radiographic Film Dosimetry for IMRT Fields in the Nearsurface Buildup Region, *J. Appl. Clin. Med. Phys.*, 2008, **9**(4), 87–97.

17 J. D. Cho, J. Son, J. Sung, C. H. Choi, J. S. Kim, H. G. Wu, J. M. Park and J. I. Kim, Flexible Film Dosimeter for in vivo Dosimetry, *Med. Phys.*, 2020, **47**(7), 3204–3213.

18 H. Sutanto, N. K. Lo, I. Alkian, P. Triadyaksa, I. Marhaendrajaya, F. Jonathan, R. Irviandi and Z. Arifin, Developing a Novel Radiosensitive Metal Ion-loaded PVA/NBT Film as Medical Low-Dose X-ray Dosimeter, *Radiat. Phys. Chem.*, 2024, **224**, 112078.

19 Q. Yang, H. Qin, L. Chen, S. Zhang, S. Mei, D. Wu, Y. Yin, X. Dai, N. Shen, Y. Tao, N. Luan, A. Jin, Y. Wang, Z. Chai, L. Sun, H. Liu and S. Wang, Metal–Organic Framework Based Thermoluminescence Dosimeter, *ACS Mater. Lett.*, 2023, **5**(6), 1619–1626.

20 L. J. Xu, X. Lin, Q. He, M. Worku and B. Ma, Highly Efficient Eco-Friendly X-ray Scintillators Based on An Organic Manganese Halide, *Nat. Commun.*, 2020, **11**(1), 4329.

21 A. M. Zeidell, T. Ren, D. S. Filston, H. F. Iqbal, E. Holland, J. D. Bourland, J. E. Anthony and O. D. Jurchescu, Organic Field-Effect Transistors as Flexible, Tissue-Equivalent Radiation Dosimeters in Medical Applications, *Adv. Sci.*, 2020, **7**(18), 2001522.

22 D. Saakshi and R. Kamaljit, Wearable Dosimeters for Medical and Defence Applications: A State of the Art Review, *Adv. Mater. Technol.*, 2021, **6**, 2000895.

23 K. Kinashi, T. Iwata, H. Tsuchida, W. Sakai and N. Tsutsumi, Composite Resin Dosimeters: A New Concept and Design for a Fibrous Color Dosimeter, *ACS Appl. Mater. Interfaces*, 2018, **10**(14), 11926–11932.

24 L. Wang, S. Guo and X. Zhang, Novel Radiochromic Elastomer Dosimeter Based on the Self-Sensitizing Effect of Disulfide Bonds, *ACS Appl. Mater. Interfaces*, 2024, **16**(5), 6474–6484.

25 M. K. Choudhary and S. Mula, Development of a BODIPY-Based Ratiometric Fluorescence off-on Dosimeter for Gamma Radiation, *New J. Chem.*, 2023, **47**, 9045–9049.

26 J. Wu, W. Liu, J. Ge, H. Zhang and P. Wang, New sensing mechanisms for design of fluorescent chemosensors emerging in recent years, *Chem. Soc. Rev.*, 2011, **40**(7), 3483–3495.

27 S. M. Al-Hazmy, Y. El-Ghoul, J. Al-Harby, H. Tar and F. M. Alminderej, Synthesis, Characterization, and Performance of Pyridomethene-BF_2 Fluorescence Dye-Doped PVA Thin Film and PVP Nanofibers as Low gamma-ray Dosimeters, *ACS Omega*, 2022, **7**(38), 34002–34011.

28 K. A. Rabaeh, A. A. Basfar and I. M. E. Hammoudeh, Novel polyvinyl alcohol film dosimeter containing 3-(4,5-Dimethylthiazol-2-yl)-2,5-diphenyltetrazolium bromide dye for high dose application, *Nucl. Eng. Technol.*, 2023, **55**(9), 3383–3387.

29 S. Feizi, Fabrication of a Flexible Polycarbonate/Porphyrin Film Dosimeter for High Dose Dosimetry, *Radiochim. Acta*, 2017, **105**(8), 657–663.

30 B. Pei, H. Su, B. Chen, W. Huang, X. Zhang, H. Miao, Y. Wang, T. Wang and G. Zhang, Quantifiable Polymeric Fluorescent Ratiometric Gamma-Ray Chemosensor, *ACS Appl. Mater. Interfaces*, 2020, **12**(37), 42210–42216.

31 Y. Qi, K. Wang and H. Zhang, Preparation and Performance Study of Radiochromic Film Dosimeter Based on Electrospinning, *Shandong Chem. Ind.*, 2023, **52**(15), 70–73.

32 P. Vo, H. Ngoc Doan, K. Kinashi, W. Sakai, N. Tsutsumi and D. Phu Huynh, X-ray Visualization and Quantification Using Fibrous Color Dosimeter Based on Leuco Dye, *Appl. Sci.*, 2020, **10**, 3798.

33 L. A. M. Migdadi, N. I. Ariffin, S. N. Nasri, L. Zhou, R. M. Ramli and N. Z. Noor Azman, Experimental Evaluation of Electrospun ZnO/WO_3/PVA-Coated Glass Nanocomposites for a Potential Radiation Dosimetry Application, *Radiat. Phys. Chem.*, 2024, **219**, 111691.

34 M. Kozicki, E. Sąsiadek, S. Kadlubowski, M. Dudek and I. Karbownik, Radiation Sensitive Polyacrylonitrile Microfibers Doped with PDA Nano-Particles, *Radiat. Phys. Chem.*, 2020, **169**, 107751.

35 P. P. Vo, H. N. Doan, K. Kinashi, W. Sakai and N. Tsutsumi, X-ray Composite Fibrous Color Dosimeter based on 10,12-Pentacosadiynoic Acid, *Dyes Pigm.*, 2021, **191**, 109356.

36 S. M. Al-Hazmy, J. Al-Harby, M. Hassan, S. Messaoudi, I. A. Alhagri and A. N. Alhakimi, A Study of the Electronic Absorption and Emission Spectra of DBDMA Dye: Solvent Effect, Energy Transfer, and Fluorescence Quenching, *J. Spectrosc.*, 2023, **2023**(1), 7802548.

37 A. Zhang, Z. Wang, W. Hong, Y. Zhang, J. Guo, Y. Wang, Y. Miao, H. Jia, H. Wang and B. Xu, Synthesis, Characterization and the Fluorescent Enhancement Mechanism of Bonded Poly(Eu(TTA)$_2$(phen)MAA-co-VA) Nanofibers by Electrospinning, *Opt. Mater.*, 2020, **106**, 110007.

38 R. K. Mishra, P. Mishra, K. Verma, A. Mondal, R. G. Chaudhary, M. M. Abolhasani and S. Loganathan,

Electrospinning Production Of Nanofibrous Membranes, *Environ. Chem. Lett.*, 2018, **17**(2), 767–800.

39 Z. Gao, X. Xiao, A. D. Carlo, J. Yin, Y. Wang, L. Huang, J. Tang and J. Chen, Advances in Wearable Strain Sensors Based on Electrospun Fibers, *Adv. Funct. Mater.*, 2023, **33**(18), 2214265.

40 L. Quoc Pham, M. V. Uspenskaya, R. O. Olekhnovich and R. A. Olvera Bernal, A Review on Electrospun PVC Nanofibers: Fabrication, Properties, and Application, *Fibers*, 2021, **9**(2), 12.

41 H. Xu, S. Yagi, S. Ashour, L. Du, M. E. Hoque and L. Tan, A Review on Current Nanofiber Technologies: Electrospinning, Centrifugal Spinning, and Electro-Centrifugal Spinning, *Macromol. Mater. Eng.*, 2023, **308**(3), 2200502.

42 A. L. Yarin, S. Koombhongse and D. H. Reneker, Taylor Cone and Jetting From Liquid Droplets in Electrospinning of Nanofibers, *J. Appl. Phys.*, 2001, **90**(9), 4836–4846.

43 C. J. Luo, S. D. Stoyanov, E. Stride, E. Pelan and M. Edirisinghe, Electrospinning Versus Fiber Production Methods: From Specifics to Technological Convergence, *Chem. Soc. Rev.*, 2012, **41**(13), 4708–4735.

44 W. Su, Z. Chang, Y. E, Y. Feng, X. Yao, M. Wang, Y. Ju, K. Wang, J. Jiang, P. Li and F. Lei, Electrospinning and Electrospun Polysaccharide-based Nanofiber Membranes: A review, *Int. J. Biol. Macromol.*, 2024, **263**, 130335.

45 H. Lian and Z. Meng, Melt Electrospinning vs. Solution Electrospinning: A comparative Study of Drug-Loaded Poly (Epsilon-Caprolactone) Fibers, *Mater. Sci. Eng., C*, 2017, **74**, 117–123.

46 H. El-Sayed, C. Vineis, A. Varesano, S. Mowafi, R. Andrea Carletto, C. Tonetti and M. Abou Taleb, A Critique on Multi-Jet Electrospinning: State of The Art and Future Outlook, *Nanotechnol. Rev.*, 2019, **8**(1), 236–245.

47 H. El-Sayed A, S. Tadao and S. Machi, Radiation-Induced Oxidative Degradation of Poly (Vinyl Chloride), *J. Appl. Polym. Sci.*, 1981, **26**(9), 2947–2957.

48 D. Qin, Y. Han and L. Hu, Enhanced X-ray Dose Response of Radio-fluorescent Hydrogels Enabled by Persulfate Salts, *J. Fluoresc.*, 2023, **33**(5), 2015–2021.

